Journal of Advanced Research in Fluid Mechanics and Thermal Sciences

Journal homepage:
https://semarakilmu.com.my/journals/index.php/fluid_mechanics_thermal_sciences/index
ISSN: 2289-7879

Numerical Study of the AP/Al/HTPB Composite Solid Propellant based Combustion Process in a Small Retro Rocket Motor

Izzat Najmi Mohd Yaacob[1], Balbir Singh[2], Norkhairunnisa Mazlan[1] , Ezanee Gires[1], Adi Azriff Basri[1], Osmera Ismail[3], Nor Afizah Salleh[3], Suraya Shahedi[3], Kamarul Arifin Ahmad[1,3,*]

[1] Department of Aerospace Engineering, Faculty of Engineering, Universiti Putra Malaysia, 43400 Serdang, Selangor, Darul Ehsan, Malaysia
[2] Department of Aeronautical and Automobile Engineering, Manipal Institute of Technology, Manipal Academy of Higher Education, Manipal 576104, Karnataka, India
[3] Science & Technology Research Institute For Defence (STRIDE), Government of Malaysia, 43000 Kajang, Selangor Darul Ehsan, Malaysia

ARTICLE INFO

Article history:
Received 1 March 2022
Received in revised form 15 May 2022
Accepted 21 May 2022
Available online 18 June 2022

Keywords:
Solid propellant; composite propellants; combustion; retro small rocket; binder; oxidizer; aluminum; nozzle

ABSTRACT

A numerical investigation of the composite solid propellant-based Combustion Process is performed to characterize the combustion behavior of ammonium perchlorate and Hydroxyl-terminated polybutadiene (HTPB) propellants in a small retro rocket motor. In this analysis, the combustion process is carried out inside the chamber with 71% oxidizer, 15% aluminum, and 14% binder. The effects of using 15% aluminum, particularly focusing on the substantially increased burning rate and composition and sizes of combustion residues are studied. A small solid-propellant-based retro rocket motor with a C-D Nozzle is studied computationally. Consistency is maintained in the boundary conditions and dimensions of the nozzle. The results clearly show a decrease in the temperature, as there is a drop in pressure along the length of the nozzle. On the other hand, due to the energy conservation, the fluid velocity marks a significant increase along the length of the nozzle. This analysis provides an outline of the combustion for small solid rocket internal flow predictions. The computation results show that the combustor carries sustained combustion throughout the process, with a steep rise in temperature near the nozzle exit. There is also a significant decrease in density near the nozzle exit due to the temperature rise. The turbulent kinetic energy also plays a major role here.

1. Introduction

The solid propellants, which are used for launch vehicles and tactical missiles, are often tailored to and classified by specific applications; each has slightly different chemical ingredients, different burning rates, different physical properties, and different performance. SRP (solid rocket propellant) is widely used in military and civilian applications [1]. In composite propellants, a heterogeneous propellant grain is formed when the oxidizer crystals and a powdered aluminum fuel are bounded strongly by a matrix of synthetic rubber (or plastic) binder, such as polybutadiene (HTPB) [1]. From a simple pipe flow to a combustion chamber, computational techniques are always useful in analyzing

* *Corresponding author.*
E-mail address: aekamarul@upm.edu.my

https://doi.org/10.37934/arfmts.96.2.98114

the end-result of these phenomena [2]. Understanding propellant combustion and internal motor ballistics are therefore critical and computational methods make it very easy to interpret [3]. According to AI-Harthi and Williams [4], ammonium perchlorate (AP) is widely used as an oxidizer in composite solid propellants and the binder plays a crucial role in the combustion process of these solid propellants [4]. A typical solid rocket manufacturing process is divided into three stages: mixing the solid propellant slurry, casting the slurry in the solid rocket motor case, and curing the solid propellant [5]. Because of their desirable mechanical and performance characteristics, AP/Al/HTPB-based solid propellants are widely used in solid rockets [6]. Solid propellants have a wide variety of applications, both military and civil. By far the most common application is in rocket engines, such as sounding rockets used for observation and launch vehicles used to place satellites in orbit [7]. Other solid propellant applications include the development of solid propellant aerosol generators (SPAGs) as alternative fire suppression systems [8]. It is difficult to model combustion in the case of a composite solid propellant. The physical inhomogeneity of the propellant, combined with a wide range of AP particle sizes, makes combustion modeling difficult. Condensed-phase heating, AP and HTPB degradation melting and surface pyrolysis, and gas-phase reactions are among the physiochemical processes that occur during the combustion of AP/HTPB propellant [9]. According to Adel and Liang [10], the mechanical properties change significantly during the aging period, but the burning rate does not change significantly. According to this research, the propellant ages via a combination of reactions such as post-cure, oxidative cross-linking, chain scission, and hydrolysis [10].

Pre-testing, in a solid-propellant rocket motor along with its essential components is not operationally possible because it results in erosion of the throat area of the nozzle. Afterward, it will jeopardize the motor performance by agglomeration of propellant particles [8]. Computational fluid dynamics thus helps to numerically evaluate the internal combustion characteristics and gives the detailed visualization of the combustion flow, thereby predicting the performance. This again helps in the performance optimization of the motor without considering the plan to fabricate and test the real rocket motors [11]. Thus, a major cost-saving can be achieved [11]. Multiphase CFD simulations also play a key role here to understand the internal ballistics [12].

A Retro Rocket Motor is made up primarily of solid or liquid propellants and a C-D nozzle. It is used to slow a vehicle down by having exhaust in the direction of motion for a short period [13]. In this paper, the SRM is assumed to be mounted on a static test stand, as shown schematically in Figure 1. In this case, the cylindrical-grain motor is constrained and comprises the aluminum weight motor casing [14]. In several cases, numerical methods are used to evaluate the simulated flow using FLUENT software. For analysis, Ansys Fluent is used, which has been used in a wide range of flow and structural problems, including in the study by Nekhamin *et al.,* [15]. Meshing is critical for achieving good simulation results. Simulation results are influenced by the mesh type and the number of divisions. Variation of the number of divisions in the mesh is used to analyze a convergent-divergent rocket nozzle. The findings revealed that the number of mesh divisions has an impact on the precision of the results. The main goal of this study is to determine the nozzle pressure, temperature, and velocity exit parameters for a turbulent k-viscous model and compare them to theoretical values. The inviscid model analysis is performed for both Air and Gas as working fluids, and theoretical values are compared. The main focus of this paper is on the relationship between combustion in the motor chamber and flow through the nozzle. As previously stated, the solid fuel combustion process differs from that of liquid fuel because the burning behaviour is dependent on the burning surface of the solid propellant grain, and this type of behaviour is examined in this paper. There are two important points to note here: the relatively slow combustion rate of aluminum droplets, in this case, results in an extended combustion zone in the chamber, and the focus of future research would be on two-

phase flow, which is difficult to design in solid rocket motors because it affects not only performance but also thermal and chemical loads on the motor components [16,17].

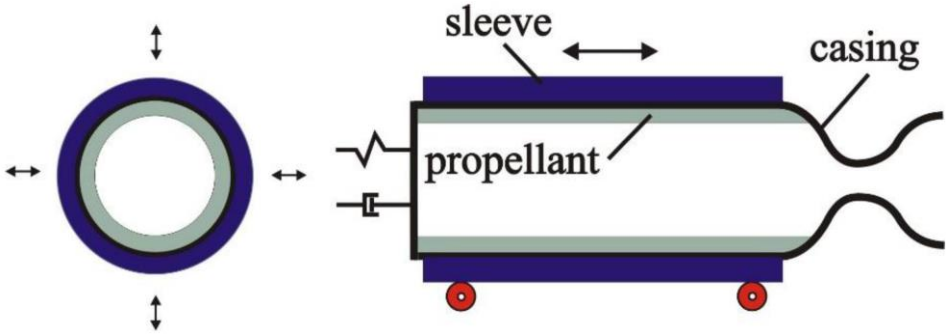

Fig. 1. The schematics of a solid-propellant rocket motor (SRM) [14]

2. Methodology

2.1 Propellant Grain Design and Performance

For grain design configuration, the cylindrical (tubular) grain core type was used in this analysis. The cylindrical core configuration can result in neutral pressure-time burning characteristics, as this is stable burning behaviour for the solid rocket propellant [1]. Figure 2(a) and Figure 2(b) depicts the cylindrical (tubular) genral configuration with progressive thrust curve with time. Besides, this type of configuration has low flexibility in the manufacturing or fabrication process of propellant grain. Figure 2(c) shows the propellant grain design, and the specification of the design has been tabulated in Table 1.

Table 1
Propellant grain design specifications

Specification	Dimension (mm)
Length, L	400
Outer diameter, D_1	45
Core diameter, D_2	20

The shape of the thrust-time curve is heavily influenced by the grain core shape. The thrust produced by a rocket motor is proportional to the burning area at any given time. This is known as the instantaneous burning area. The specification of the propellant grain has been transferred in the BurnSim software which is a solid propellant internal ballistics simulation and research rocket motor design software to get the theoretical performance data. The propellant grain performance data gain in the BurnSim software is calculated based on the propellant grain specification such as the grain length, outer diameter, and core diameter. The *Kn* factor is defined as the ratio of the propellant burn area to the nozzle throat area. Take note that *Kn* is a time-varying, instantaneous value that alters as the propellant burns. During the total burn time of the motor, the *Kn* may increase or decrease (or both) depending on the grain geometry. The initial *Kn* is significant because it influences the motor's ability to ignite. The maximum *Kn*, also known as the peak *Kn*, is significant because it is proportional to the peak chamber pressure. All of this can be easily calculated using rocket motor simulators and design tools like BurnSim. The propellant grain cross-section of the burning surface is shown in Figure 2(d) and the simulation performance data using Burnsim software of the propellant grain is tabulated in Table 2.

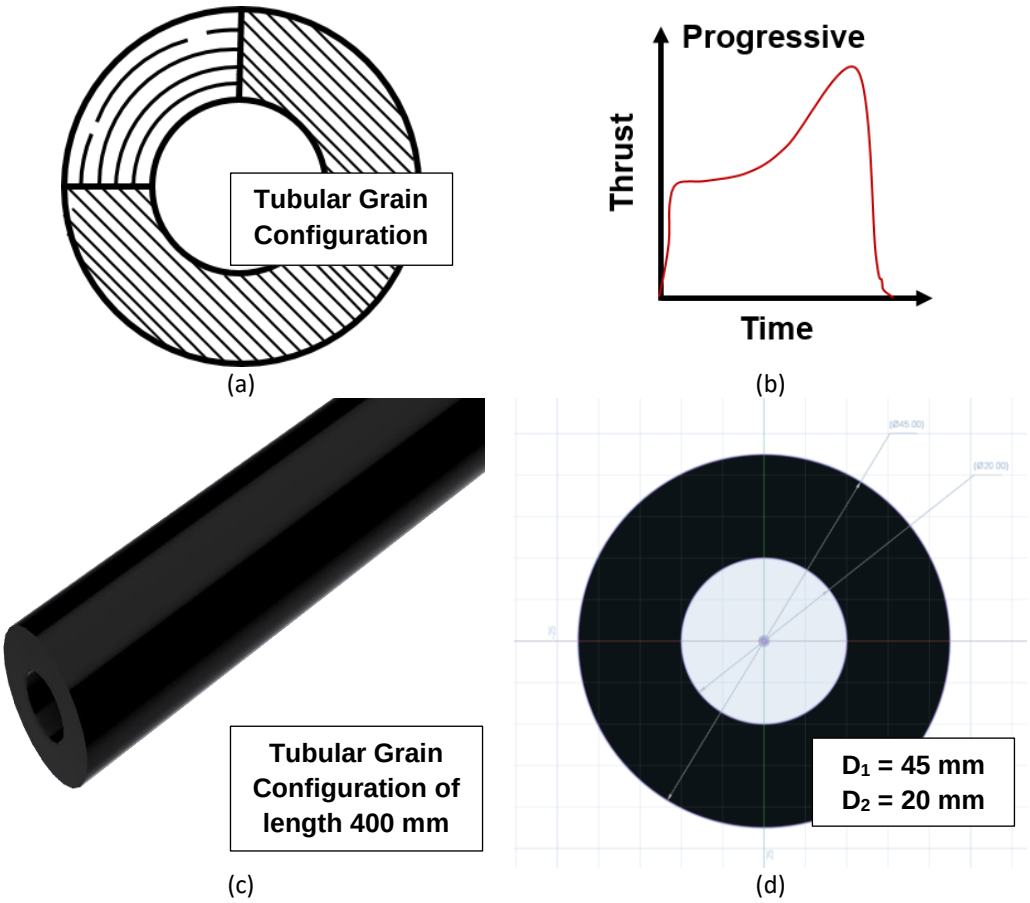

Fig. 2. (a) Cylindrical (tubular) propellant grain configuration, (b) Progressive thrust curve for the tubular grain geometry, (c) Cylindrical propellant grain configuration used here, (d) Propellant core cross-section

Kn needs to be controlled when designing motors and the best and the primary way to control the overall *Kn* curve for a standard motor design is by choosing the grain geometry. Other factors are the surface area of the propellant, the nozzle throat diameter, etc.

Table 2
Propellant grain performance data from BurnSim

Parameter	Value
Initial Kn	152
Max Kn	294
Maximum chamber pressure	4078.4 Kpa
Volume loading	82.6%
Port/Throat area	1.93
Core L/D ratio	17.3
Propellant mass	3.741 lbs
Burn time	3.47 s
Total impulse	2111 Ns
Motor class	K-608

Figure 3 shows the data of *Kn* versus time plotted in a graphical format. As the process progresses from the start of the burning until 36 seconds, the propellant grain exhibits neutral burning characteristics.

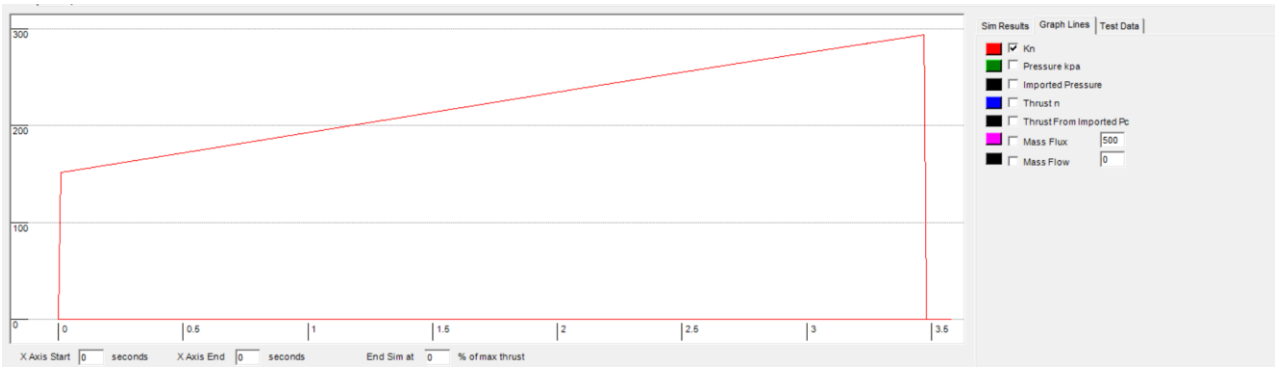

Fig. 3. The factor Kn versus time plot from BurnSim shows burning characteristics

2.2 Rocket Motor Chamber and Nozzle Design

The rocket motor chamber was used to simulate the burning flow of the propellants because the propellant grain is loaded in this chamber, which is directly connected to the nozzle. The analysis follows the design and dimension closer to the study by Sabnis [16] for the analysis and validation. At the initial grain configuration, the geometry was similar to the super ballistics test motor as in the study by Sabnis [16]. In these calculations, the propellant contained 15% aluminum by weight. Figure 4 depicts a schematic of the motor geometry, and Table 3 lists the rocket motor design specifications.

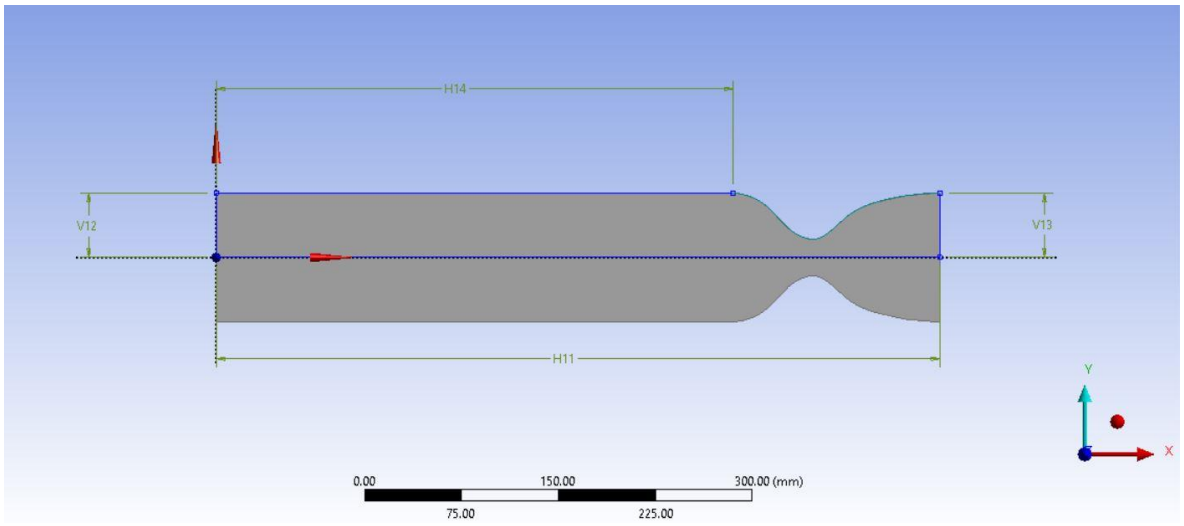

Fig. 4. Schematics of the motor geometry

Table 3
Rocket motor design specifications

Specification	Dimension(s)
Motor chamber radius (V12)	50 mm
Motor chamber length (H14)	466 mm
Convergent nozzle angle (A18)	32°
Divergent nozzle angle (H4)	48°
Throat radius (H22)	15 m
Nozzle exit radius (H28)	50 mm

The nozzle is an important component of the rocket motor because it is where the exhaust gases are pushed out of the chamber. The throat separates the general design of the rocket nozzle, which is usually converged-diverged. The spiral nozzle is also converged-diverged, but the exit chamber has

a spiral flute shape. Because of its stability, the spiral-type nozzle was chosen for the study. The nozzle design with dimensions is shown in Figure 5(a), and the exhaust chamber dimension is shown in Figure 5(b). Table 4 shows the rocket nozzle design specifications.

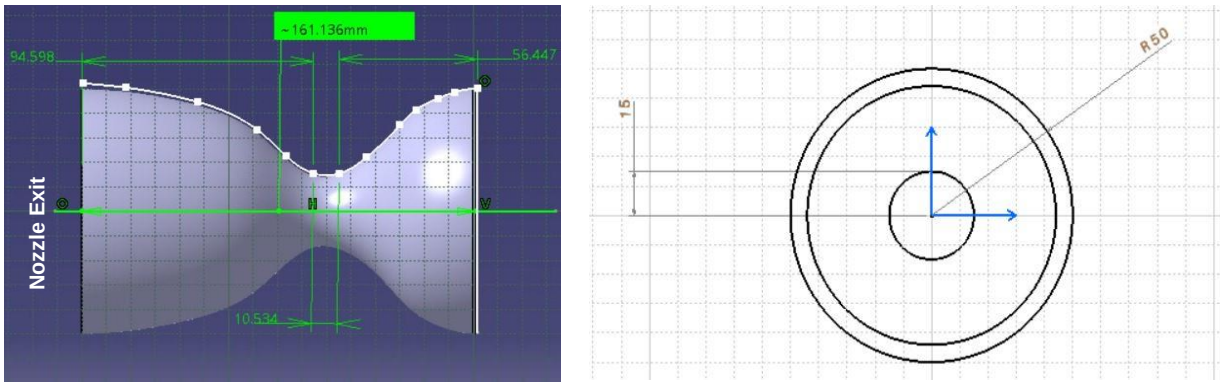

(a) (b)

Fig. 5. Rocket nozzle design and dimension of (a) cross-section and (b) exhaust chamber

Table 4
Rocket nozzle design specifications

Specification	Dimension(s)
Nozzle total length	161 mm
Convergence length	95 mm
Divergence length	56 mm
Nozzle divergence angle	48°
Chamber inside diameter	100 mm
Nozzle exit diameter	100 mm
Throat length	11 mm
Throat diameter	30 mm

2.3 Propellants Used and their Properties

Solid rocket propellant has many types of configurations for example single-based, double-based, and composite types propellant. All of these types of propellants have their performance and criteria. The composite type with AP/Al-based is chosen in this study. This type of propellant is widely being used for the missile rocket for military applications. One of the advantages of using AP as an oxidizer in the composite propellant is it can produce high thrust with a high burn rate compared to other materials. In this paper, we attempt to reduce the complex physics involved in order to develop a thorough model for the combustion chamber of a solid rocket motor (SRM). Because of the intricacy and computing cost, surface reactions, melting and other complicated metal particle combustion processes are not explored.

The solid propellant used in this research is heterogeneous propellant which consists of solid oxidizer particles Ammonium Perchlorate (AP) 71%, metallic fuel particle Aluminum (Al) powder 15%, dispersing in HTPB polymeric binder matrix as shown in Table 5 [10]. AP/Al propellant is the ester-based, as it is bound with an ester type of binder. The most common ad compatible type of ester binder for this kind of propellant based is Hydroxyl-terminated polybutadiene. This ester can form a 3D structure of cross-linkage that can form a matrix for the oxidizer and fuel. Besides, HTPB also can produce good mechanical and thermal properties to the propellant grain although the condition of the propellant grain is influenced by the manufacturing process.

Table 5
Propellant data and specifications [16]

Property	Propellant	Value
Composition	Ammonium Perchlorate (AP)	71 %
	Binder (HTPB)	14 %
	Aluminum (AL)	15 %
Density		1764.6 kgm^{-3}
Burn Rate		9.0678×10^{-3} m/s

2.4 Mathematical Model and Numerical Process

For mathematical modeling, an SRM is defined as a cylindrical, circular duct with a circumferential porous surface that is canted at an angle [18]. The schematics of a typical retro solid rocket motor are included in Figure 6(a) and it shows the outer components of SRM. As shown in Figure 6(b), the coordinate system's origin is at the interface, where z and r denote the axial and radial coordinates, respectively [18]. The cylindrical motor's non-tapered section has dimensions of length L and radius R. While there is a radial velocity component at the interface, it is important to note that it does not contribute to mass traverse into the tapered region.

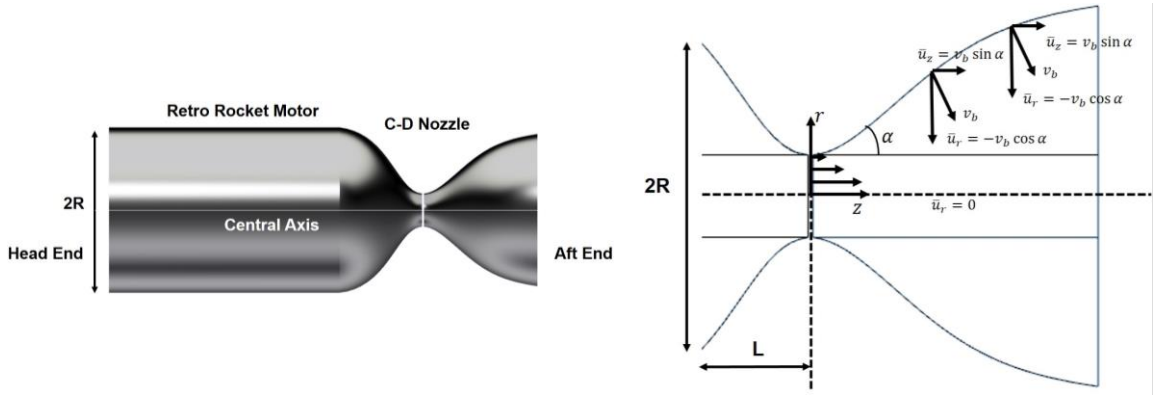

(a) (b)

Fig. 6. (a) Schematics of a typical retro solid rocket motor, (b) physical boundary conditions for modeling [18]

As per Sams IV *et al.,* [18], the scalar kinematic equations of motion can therefore be written as in Eq. (1) to Eq. (3)

$$\bar{u}_r \frac{\partial \bar{u}_r}{\partial r} + \bar{u}_z \frac{\partial \bar{u}_r}{\partial z} = -\frac{1}{\rho}\frac{\partial \bar{p}}{\partial r} \tag{1}$$

$$\bar{u}_r \frac{\partial \bar{u}_z}{\partial r} + \bar{u}_z \frac{\partial \bar{u}_z}{\partial z} = -\frac{1}{\rho}\frac{\partial \bar{p}}{\partial z} \tag{2}$$

$$\bar{\Omega} = \bar{\Omega}_\theta = \frac{\partial \bar{u}_r}{\partial z} - \frac{\partial \bar{u}_z}{\partial r} = -\frac{1}{r}\frac{\partial^2 \bar{\Psi}}{\partial z^2} - \frac{\partial}{\partial r}\left(\frac{1}{r}\frac{\partial \bar{\Psi}}{\partial r}\right) \tag{3}$$

where $\bar{u}_r$ and $\bar{u}_z$ are defined in terms of vorticity factor Ψ as in Eq. (4)

$$\bar{u}_r = -\frac{1}{r}\frac{\partial \bar{\Psi}}{\partial z} \text{ and } \bar{u}_z = -\frac{1}{r}\frac{\partial \bar{\Psi}}{\partial r} \tag{4}$$

The physical boundary conditions then can mathematically be obtained as in Eq. (5) (v_b is the injection velocity)

$$\begin{aligned} &at\ z = 0;\ \bar{u}_z = \pi v_b (L/R)\cos(\pi r^2/R^2) \\ &at\ r = r_s;\ \bar{u}_z = v_b \sin\alpha \\ &at\ r = r_s;\ \bar{u}_r = -v_b \cos\alpha \\ &at\ r = 0;\ \bar{u}_r = 0 \end{aligned} \tag{5}$$

The general setup with the pressure-based solver type was used in this study for the rocket motor analysis using ANSYS FLUENT academic version available at UPM, Malaysia. The energy equation was then turned on to ensure that all of the chemical reaction equations could be applied to process the combustion analysis for the rocket motor. Furthermore, the analysis model uses non-premixed species as the mixture for the material, which was entered using a pdf mixture template. The materials assigned in the rocket motor propellant composition have also been set up in the mixture template pdf input. With a maximum of 1500 iterations, the setup process was initialized relative to the cell zone. For all equations, explicit under-relaxation factors of 0.1 are used. However, these settings may differ for optimal convergence performance and solution speed-up for other software and are only provided as a guide. For the formation of the flamelet library file from CHEMKIN mechanism files, one of the methods is the default non-adiabatic approach implemented in Fluent [19]. This will be used for future analysis. Table 6 lists the inlet boundary conditions (initial values of parameters) used in the analysis.

Table 6
Boundary conditions used in this study to evaluate the performance

Parameter	Value
Inlet velocity	298.98 m/s
Initial gauge pressure	7890 kPa
Inlet turbulence specific method	K and Omega
Inlet temperature	300 K
Gauge pressure	0 Pascal
Backflow direction specification method	Normal to boundary
Outlet turbulence specification method	K and Omega
Backflow total temperature	5000 K
No. of iteration	1500 iterations

2.5 Meshing and Grid Independent Study

According to the computational scope, the distribution of the surface grid points was determined by the degree of resolution required in different areas near the module and the front, such as the area near the throat and beyond. Figure 7 shows a close-up view of the semi-structured 3D mesh on the surface of the module (SRM). A solution-adaptive approach has been used to refine grids in high gradient regions of the areas of interest. Figure 8(a) and Figure 8(b) depict the rocket motor computational domain and grid for the inlet chamber and the nozzle throat area.

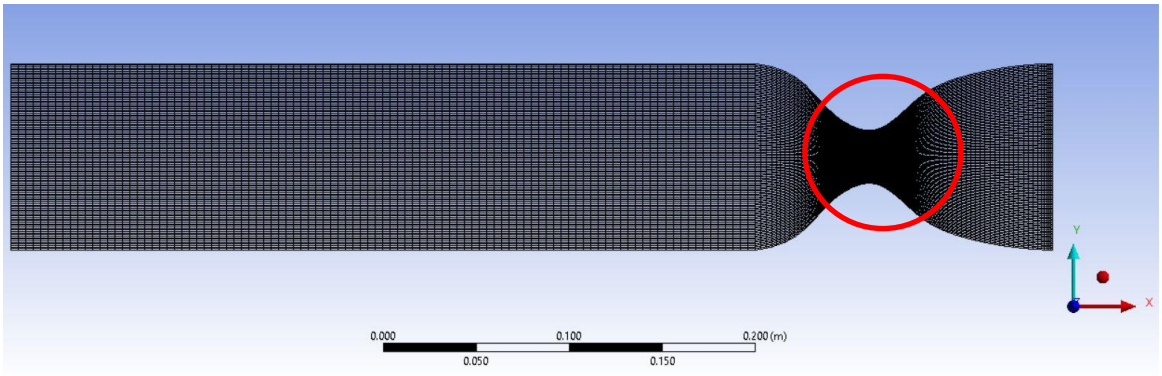

Fig. 7. Rocket motor computational domain and grid

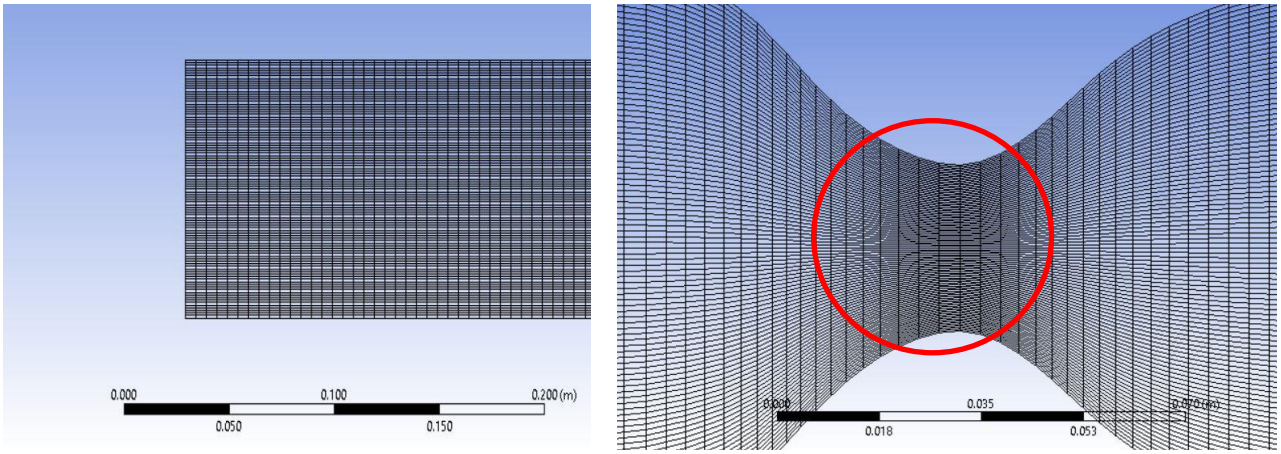

(a) (b)

Fig. 8. Rocket motor computational domain and grid (a) inlet chamber, (b) nozzle throat area

First, a grid independence study must decide the 'right' mesh size chosen in the numerical simulations. Generally, for capturing variations in flow properties, a denser mesh is favored and is more attractive. A very fine mesh or dense mesh, however, requires significantly greater computer resources and time [2]. By performing this grid independence study, a consensus is found, and the outcomes can be seen. In Table 7, the meshing characteristics of the various levels of mesh sharpness can be found. As medium and fine meshes are applied, it can be seen that the variation of the velocity value at a specifically chosen location x = 1.7 m, is much more considerable than that predicted by using a coarser mesh. There is no significant difference between the medium and fine mesh.

Table 7
Grid independent study parameters

Mesh number (No of the division each edge size)	Number of nodes	Number of elements	Velocity (at point x=0.25 m) m/s
1 (120, 100, 70, 70)	20933	20640	8.10
2 (110, 90, 60, 60)	16352	16103	6.50
3 (100, 80, 50, 50)	13534	13300	6.15
4 (90, 70, 40, 40)	11446	11192	4.20

Along the combustor wall, a low-Re mesh criterion for the non-dimensional wall distance $y+\leq 1$ is fulfilled. To save computational resources, a total grid size of 16352 nodes and 13534 elements (2nd grid) was used based on a preliminary mesh convergence study shown in Table 7. Grid 2 and Grid 3 have no significant differences in velocity.

2.6 Validation of the Current Numerical Method

To see the variation in parameters from chamber to nozzle exit, numerical contours from this computational analysis were compared with Ecker *et al.,* [17], a comparable prior work. It has been discovered that practically all of the parameters exhibit a similar tendency. The comparison exhibited in for temperature contours is provided. Interphase energy transfer reduces streamwise rates and raises static temperatures, particularly near the wall [17].

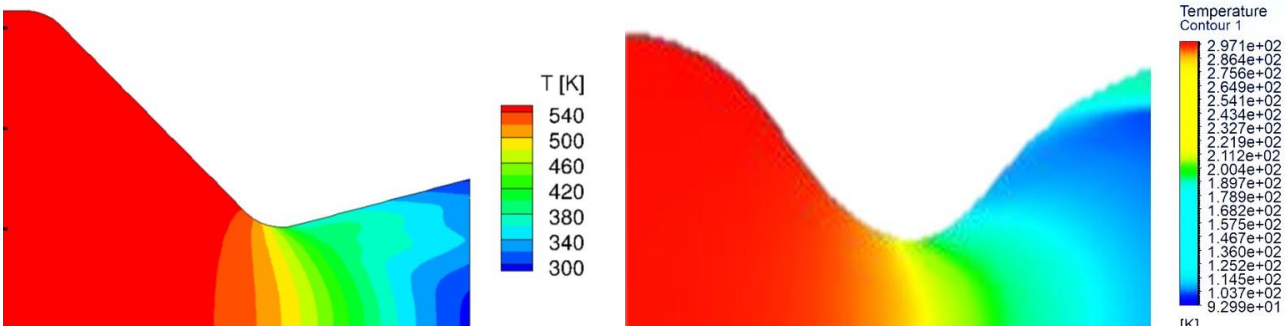

(a) (b)

Fig. 9. Comparison of temperature contours (a) from Ecker *et al.,* [17], (b) current numerical analysis

Figure 9(a) and Figure 9(b) show a comparison of the current computation and data from Ecker *et al.,* [17] for temperature contours. While there are minor changes between the single and two phase numerical computations, the results compare favourably with a nearly same trend.

3. Results and Discussion

The simulation of flow combustion is performed under steady-state conditions. Contours of pressure, temperature, density, velocity, and turbulent kinetic energy are obtained. The average values of the parameters at the nozzle exit plane are noted. In this section, the variations in pressure, temperature, velocity, and other parameters are discussed. It is important to note here that the propellant combustion process depends upon the mixing of the propellants. For example, oxidizer particle size distributions and quantity play a significant role.

3.1 Velocity Magnitude During the Process

The velocity contours for this numerical model analysis are shown in Figure 10. It shows the increase in exhaust velocity when compared to the chamber velocity. Close-ups of the velocity contours at the nozzle exit and how velocity varies from chamber to nozzle exit are shown in Figure 11(a) and Figure 11(b) respectively. The combustion analysis shows the overall combustion of the AP/binder and aluminum at the propellant surface, as well as complete reactions that result in an increase in velocity at the middle of the head end.

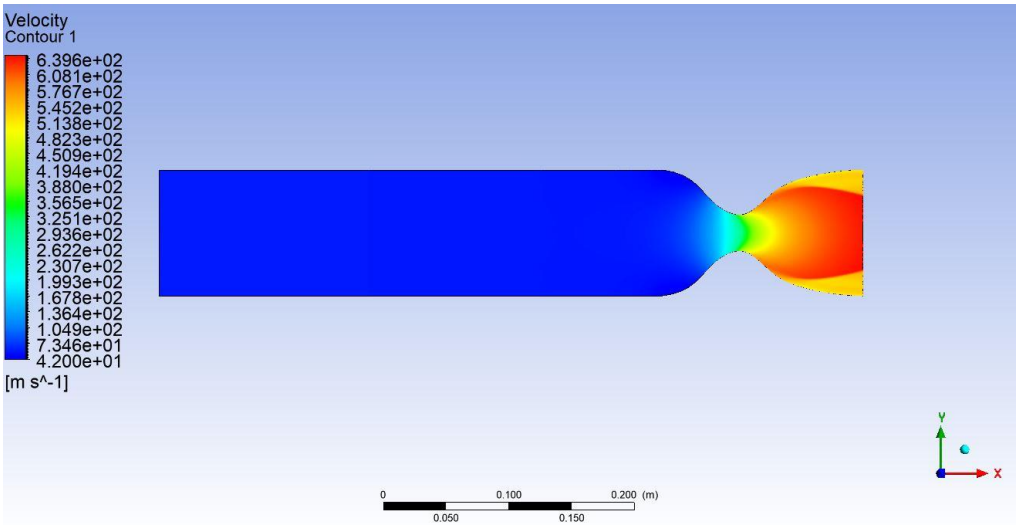

Fig. 10. Velocity contour of the numerical analysis of the SRM

Velocity contours reveal that the velocity field changes substantially at the exit. For this reacting case, the maximum velocity of 640 m/s is observed as exhaust at the exit of the nozzle for this small retro thruster. The heat released from the chemical reaction makes the significant areas of flow subsonic in the case of non-reacting. The case is different at the combustor exit when combustion takes place. The computation results show that the combustor carries sustained combustion throughout the process within the combustor for the inlet and geometry conditions.

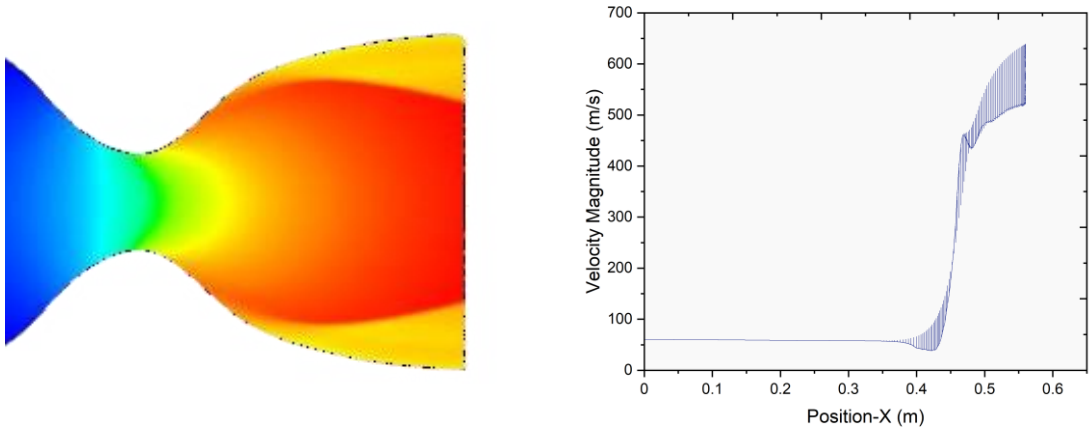

(a) (b)

Fig. 11. (a) Close up of the velocity contour at nozzle exit, (b) velocity magnitude versus position

3.2 Pressure Distribution Across the Chamber and Nozzle During the Process

The Pressure contour generated is shown in Figure 12. From the simulation results, it is revealed that the expansion of flow is very optimum in the C-D nozzle. Close-ups of the pressure contours at the nozzle exit and how pressure varies from chamber to nozzle exit are shown in Figure 13(a) and Figure 13(b) respectively. From the convergent section to the exit plane of the divergent section, the pressure decreases. This indicates that no shock has formed inside the nozzle. The static and total pressures in the combustion chamber are measured. The pressure in a non-reacting flow is much

higher, whereas the pressure in a reacting flow is much higher due to the chemical species reaction and products.

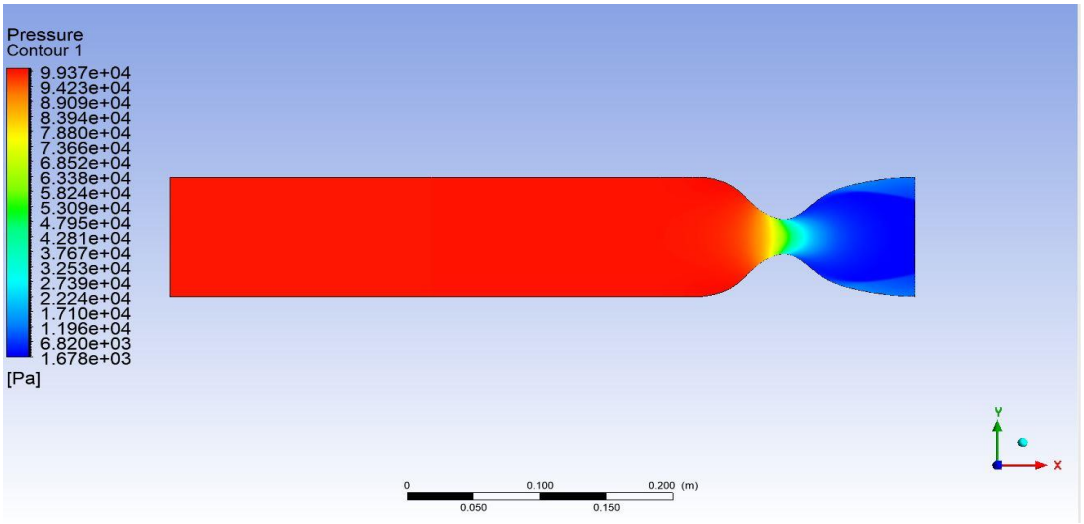

Fig. 12. Pressure contour of the numerical analysis of the SRM

The pressure drop to around 1.68 kPa near the end of the divergent part is obvious from the contour, which explains the significant increase in exhaust velocity and gas expansion, and then again takes its lead. All this is due to the chemical kinetics involved in the combustion process.

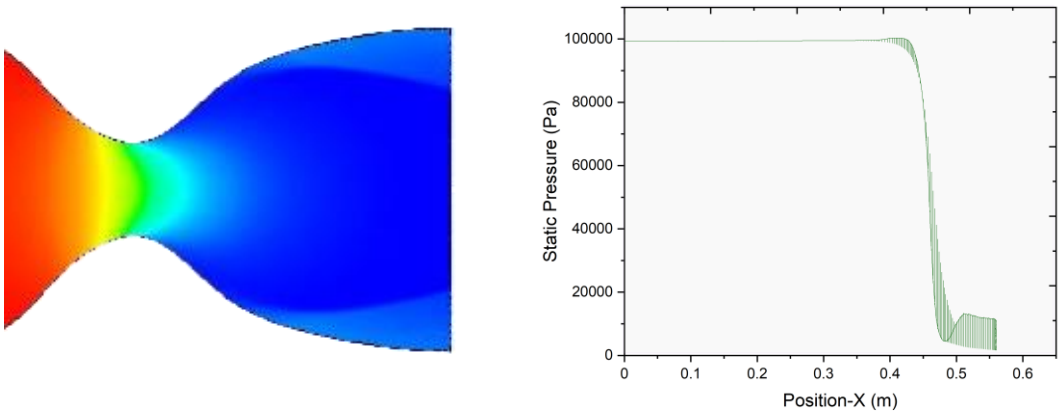

(a) (b)

Fig. 13. (a) Close up of the pressure contour at nozzle exit, (b) pressure variation versus position

3.3 Temperature Effect During the Process

Figure 14 shows the temperature distribution of the reacting flow field. The propellant surface temperature is 260 K (the AP/binder flame temperature) and rises to nearly 300 K in the core due to aluminum combustion and then drops to 100 K near the exit. Close-ups of the temperature contours at the nozzle exit and how temperature varies from chamber to nozzle exit are shown in Figure 15(a) and Figure 15(b) respectively. There are signs that the temperature in the head end region is slightly higher. This is due to the low velocities in this area, which prevent the burning particles from being swept away, resulting in local particle hot regions. The computation results show that the combustor carries sustained combustion throughout the process, with a steep fall in temperature near the

nozzle exit. Chemical reactions and lateral heat transfer from the flame also heat the area between the wall and the fame center. The temperature at the combustor axis is nearly unchanged.

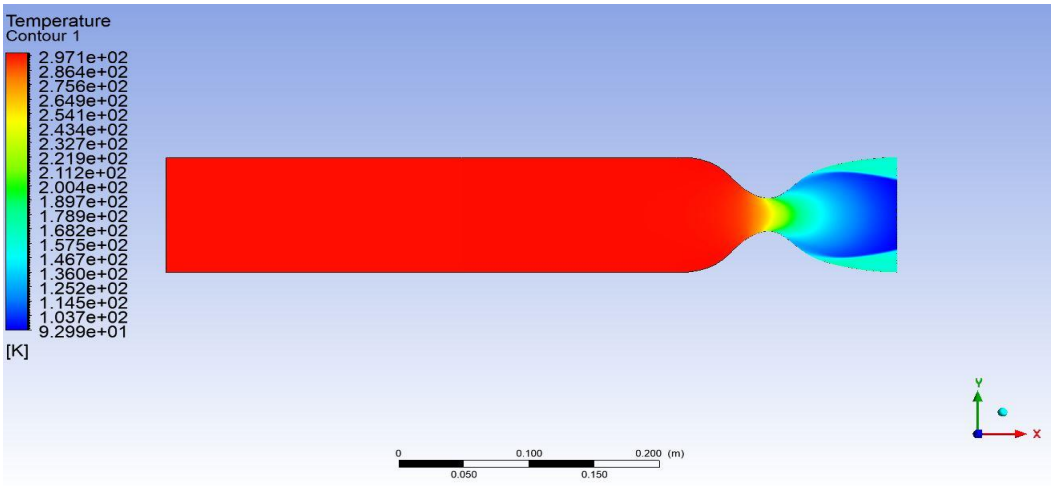

Fig. 14. Temperature contour of the numerical analysis of the SRM

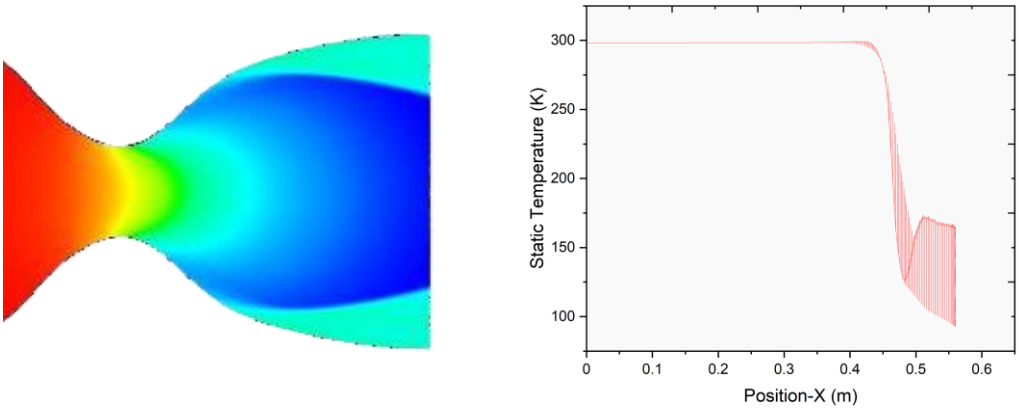

(a) (b)

Fig. 15. (a) Close up of the temperature contour at nozzle exit, (b) temperature variation versus position

3.4 Density Across the Chamber and the Nozzle During the Process

The density distribution of the reacting flow field is presented in Figure 16. Close-ups of the density contours at the nozzle exit and how density varies from chamber to nozzle exit are shown in Figure 17(a) and Figure 17(b) respectively. Here it is important to note that the movement of aluminum droplets at the propellant surface undergoes combustion, which enhances the aluminum mass fraction (not calculated here).

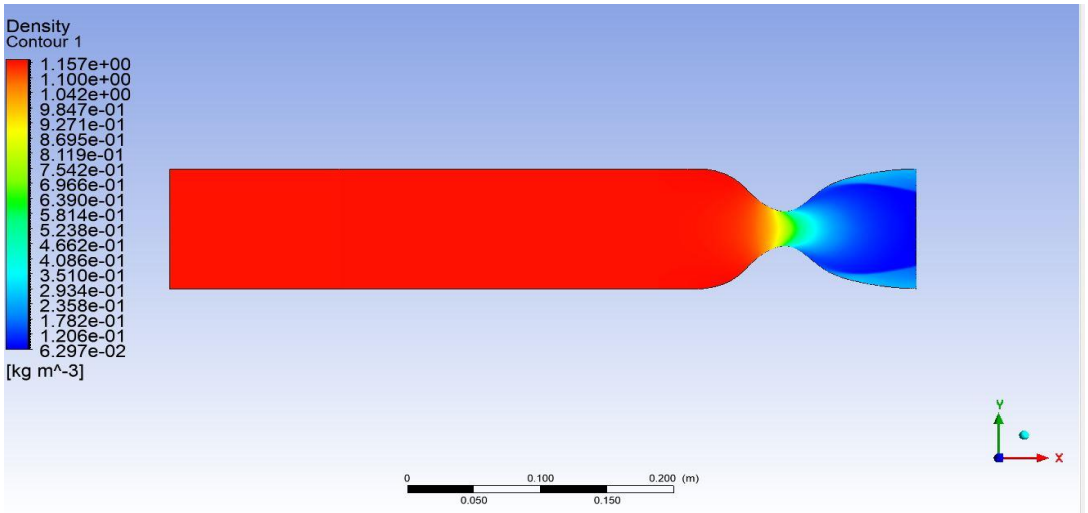

Fig. 16. Density contour of the numerical analysis of the SRM

It is important to understand that what affects the density is the distributed combustion of aluminum, and this effect can be seen in Figure 17(a). The motor chamber density is fairly uniform (approximately 1.16 kg/m^3), whereas the density at the propellant surface is approximately 0.66 kg/m^3 near the nozzle throat and drops to about 0.06 kg/m^3 near the exit region because of the rise in veocity as a result of this distributed combustion and cross section area. Here also, the computation results show that the combustor carries sustained combustion throughout the process and can exist within the combustor. This diffusion with a maximum temperature might be, adding significant heat to the flow.

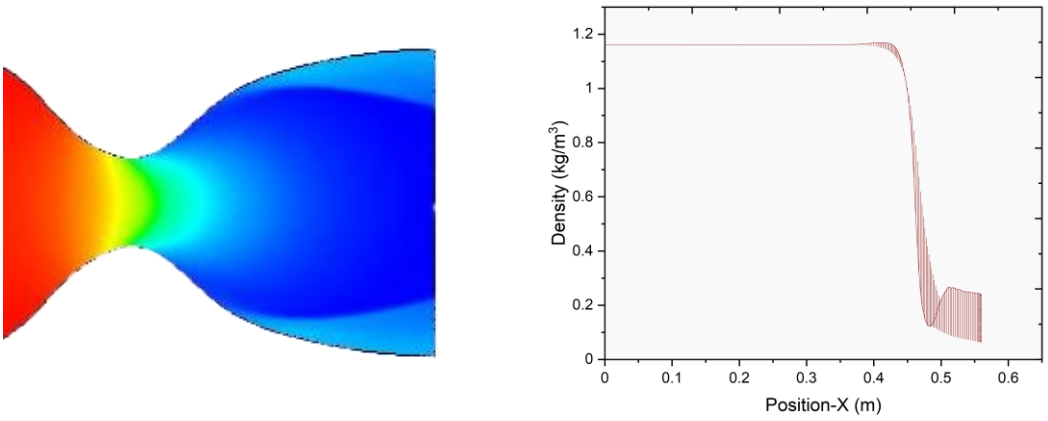

(a) (b)

Fig. 17. (a) Close up of the density contour at nozzle exit, (b) density variation versus position

3.5 Mach Number Variation across the Chamber and the Nozzle Exit

Mach number ariation across the chamber is presented in Figure 18. Close-ups of the Mach contours at the nozzle exit and how Mach varies from chamber to nozzle exit are shown in Figure 19(a) and Figure 19(b) respectively. The Mach number, which is a ratio of gas velocity to sound velocity, is increasing from stagnant condition to Mach 3.3 at the nozzle exit. This is due to the fact that there is a substanstial increase in exhaust velocity in the nozzle as well as reduction in sound velocity. The flow is clearly subsonic in the convergent part, sonic at the throat and supersonic in the

divergent part of the nozzle. The thrust developed by the nozzle increases with increase in exit velocity.

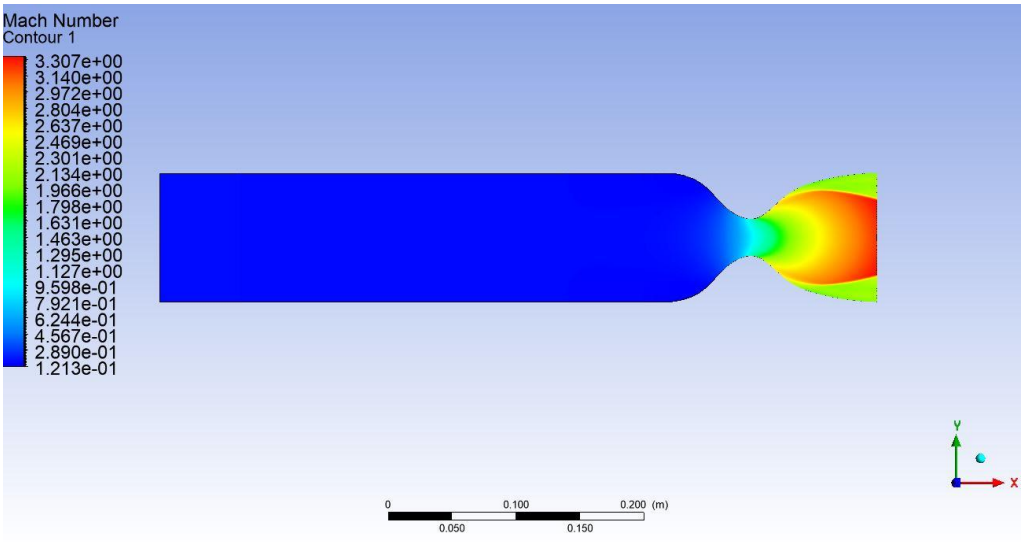

Fig. 18. Mach contour of the numerical analysis of the SRM

As we can see from the increased bubble in the exit area, the turbulent kinetic energy is not well captured in this analysis. This is because the positive dilatation rate due to thermal expansion is not properly captured here, causing the turbulent kinetic energy transport to be affected. This means that the rate of dilation and the resulting pressure gradient is crucial.

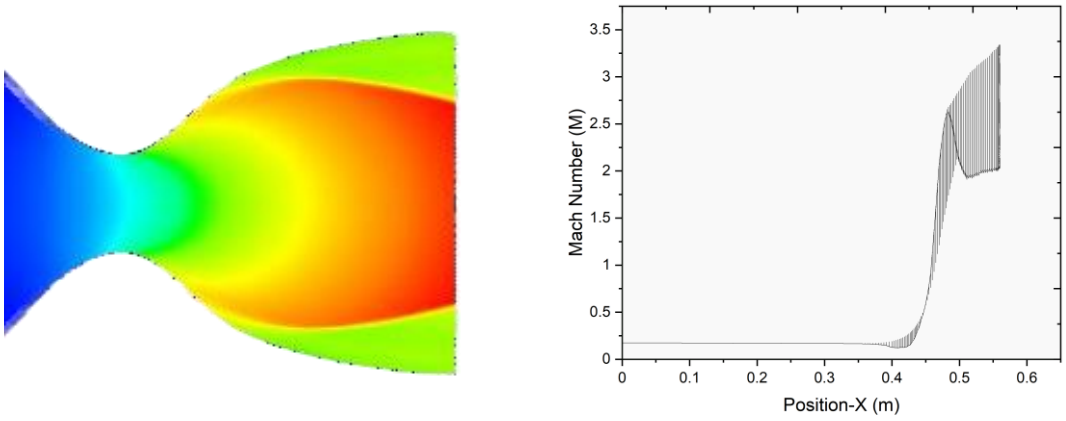

(a) (b)

Fig. 19. (a) Close up of the Mach contour at nozzle exit, (b) Mach variation versus position

The computations show that there is a sustained kinetic energy at a low value within the combustor. TKE has a relationship with exhaust vorticity due to self-induced pressure gradient, and thus accounts for the characteristic nature of turbulence. A high-fidelity CFD simulation with experimental analysis is required.

It is important to highlight that the current study is a simple steady state analysis, and that the comprehensive unsteady analysis is preferable for gaining a better understanding of real solid propellant combustion. In the future, such approach can be used to study a few crucial issues. For example, it is generally accepted that thermal breakdown happens inside the solid when the surface

heats up. However, due to the high activation energy of this process, it is frequently thought that the pyrolysis is confined in an infinitely thin zone at the surface, while the propellant remains inert [14]. To understand complex processes such as the development of thin layers of gaseous bubbles in the combustion process of these AP-based soild propellants already explored experimentally, numerical computations should be able to emphasise temporal integration of a series of semi-discretized equations [14]. Capturing dynamic through high-order techniques, comprehensive gas kinetics, and dynamic time step variations are only a few of the strategies used to ensure a thorough grasp of complex unsteady phenomena.

4. Conclusions

After designing the grain, motor, and exit nozzle, an analysis in ANSYS FLUENT is performed and discussed to simulate the internal flow in small retro solid rocket motors with metalized propellants. The results of the calculations show that the analysis can realistically simulate the combustion of aluminum in small solid rocket motors. The numerical calculations with a 15% aluminum propellant show that this composition transits from its initial state (referring to AP/binder) to its final state (referring to peak aluminum mass fraction) over an extended combustion region in the chamber. While the flow fields are generally identical up to the throat area, the diverging nozzle section exhibits significant variances. The results clearly show that as the pressure decreases along the length of the nozzle, so does the temperature. However, due to energy conservation, the fluid velocity increases along the length of the C-D nozzle. In the future, this analysis will require data on the particle size distribution at the propellant surface, the fraction of metal that burns at the surface, and so on. Additional experiments aimed at gathering these data would be beneficial in validating the analysis. The analysis can also be used to effectively plan experiments and interpret the results of those experiments.

Acknowledgment

The authors gratefully acknowledge the contributions of FAAS ENGINEERING AND CONSULTANCY SDN. BHD in providing opportunities to flourish and make engineering and energy related research a reality through the grant no: 6300248. The authors would also like to convey their gratitude to UPM for providing the necessary facilities required for this research work.

References

[1] Sutton, George P., and Oscar Biblarz. *Rocket propulsion elements*. John Wiley & Sons, 2016.
[2] Singh, Balbir, Usman Ikhtiar, Mohamad Firzan, Dong Huizhen, and Kamarul Arifin Ahmad. "Numerical Analysis of a Mobile Leakage-Detection System for a Water Pipeline Network." *Journal of Advanced Research in Fluid Mechanics and Thermal Sciences* 87, no. 1 (2021): 134-150. https://doi.org/10.37934/arfmts.87.1.134150
[3] Davenas, Alain, ed. *Solid rocket propulsion technology*. Pergamon, 1992.
[4] Al-Harthi, A., and A. Williams. "Effect of fuel binder and oxidiser particle diameter on the combustion of ammonium perchlorate based propellants." *Fuel* 77, no. 13 (1998): 1451-1468. https://doi.org/10.1016/S0016-2361(98)00059-3
[5] Iwasaki, Akihiro, Kotaro Matsumoto, Ryosuke Ban, Shun Yoshihama, Taro Nakamura, and Hiroto Habu. "The continuous mixing process of composite solid propellant slurry by an artificial muscle actuator." *Transactions of the Japan Society for Aeronautical and Space Sciences, Aerospace Technology Japan* 14, no. 30 (2016): 107-110. https://doi.org/10.2322/tastj.14.Pa_107
[6] Jarocki, Christopher M., Timothy D. Manship, and Steven F. Son. "Investigation of Mechanical Properties of AP/Al/HTPB-Based Propellants using 2-D Digital Image Correlation at Large and Small Scales." In *AIAA SCITECH 2022 Forum*, p. 1896. 2022. https://doi.org/10.2514/6.2022-1896
[7] Lysien, Kinga, Agnieszka Stolarczyk, and Tomasz Jarosz. "Solid Propellant Formulations: A Review of Recent Progress and Utilized Components." *Materials* 14, no. 21 (2021): 6657. https://doi.org/10.3390/ma14216657

[8] Richter, Elizabeth, and Ulrich Krause. "Development of solid propellant for the production of fire suppression aerosols." *Fire Safety Journal* 120 (2021): 103113. https://doi.org/10.1016/j.firesaf.2020.103113
[9] Cai, Weidong, Piyush Thakre, and Vigor Yang. "A model of AP/HTPB composite propellant combustion in rocket-motor environments." *Combustion Science and Technology* 180, no. 12 (2008): 2143-2169. https://doi.org/10.1080/00102200802414915
[10] Adel, Walid M., and Guozhu Liang. "Service life prediction of AP/Al/HTPB solid rocket propellant with consideration of softening aging behavior." *Chinese Journal of Aeronautics* 32, no. 2 (2019): 361-368. https://doi.org/10.1016/j.cja.2018.08.003
[11] Al Mayas, A. A., Chen Aolin, Faieza Abdul Aziz, Noorfaizal Yidris, and Kamarul Arifin Ahmad. "Investigation of Solid Propellant Rocket Motor Nozzle via CFD Simulation." *Journal of Advanced Research in Fluid Mechanics and Thermal Sciences* 68, no. 2 (2020): 1-8. https://doi.org/10.37934/arfmts.68.2.18
[12] Bougamra, Ahmed, and Huilin Lu. "Multiphase CFD simulation of solid propellant combustion in a small gun chamber." *International Journal of Chemical Engineering* 2014 (2014). https://doi.org/10.1155/2014/971808
[13] Hemanth, Varada Anil, and U. S. Jyothi. "CFD Analysis of a Solid Propellant Retro Rocket Motor using Ansys Fluent." In *E3S Web of Conferences*, vol. 184, p. 01054. EDP Sciences, 2020. https://doi.org/10.1051/e3sconf/202018401054
[14] Greatrix, David. "Numerical evaluation of the use of aluminum particles for enhancing solid rocket motor combustion stability." *Energies* 8, no. 2 (2015): 1195-1215. https://doi.org/10.3390/en8021195
[15] Nekhamin, Mark, Ihor Beztsennyi, Natalia Dunayevska, and Volodimir Vyfatnuik. "On Using the ANSYS FLUENT Software for Calculating the Process of Burning a Mixture of Particles From Different Types of Solid Fuels." *Eastern-European Journal of Enterprise Technologies* 4, no. 8 (106) (2020): 48-53. https://doi.org/10.15587/1729-4061.2020.209762
[16] Sabnis, Jayant S. "Numerical simulation of distributed combustion in solid rocket motors with metalized propellant." *Journal of Propulsion and Power* 19, no. 1 (2003): 48-55. https://doi.org/10.2514/2.6101
[17] Ecker, Tobias, Sebastian Karl, and Klaus Hannemann. "Modeling of aluminum particle combustion in solid rocket combustion chambers." In *53rd AIAA/SAE/ASEE Joint Propulsion Conference*, p. 4781. 2017. https://doi.org/10.2514/6.2017-4781
[18] Sams IV, Oliver C., Joseph Majdalani, and Tony Saad. "Mean flow approximations for solid rocket motors with tapered walls." *Journal of Propulsion and Power* 23, no. 2 (2007): 445-456. https://doi.org/10.2514/1.15831
[19] Strokach, Evgeny, Victor Zhukov, Igor Borovik, Andrej Sternin, and Oscar J. Haidn. "Simulation of a GOx-GCH4 Rocket Combustor and the Effect of the GEKO Turbulence Model Coefficients." *Aerospace* 8, no. 11 (2021): 341. https://doi.org/10.3390/aerospace8110341